Far-infrared Galaxy Evolution Surveys with *Herschel*

Dieter Lutz[1]

[1]*Max-Planck-Institut für extraterrestrische Physik, Germany*

ABSTRACT

The 2009-2013 mission of the *Herschel Space Observatory* has dramatically enhanced our ability to use dust-reradiated far-infrared emission in the context of multiwavelength studies of galaxy evolution. Near its peak, three quarters of the cosmic infrared background are now resolved into individually detected sources. The use of far-infrared diagnostics of dust-obscured star formation and of interstellar medium conditions has expanded from rare extreme high-redshift galaxies to more typical main sequence galaxies and hosts of active galactic nuclei, out to $z \gtrsim 2$. These studies shed light on the evolving role of steady equilibrium processes and of brief starbursts, at and since the peak of cosmic star formation and black hole accretion.

1. A RESOLVED VIEW OF THE COSMIC FAR-INFRARED BACKGROUND

Since the first indications for an evolving population of infrared galaxies found in *IRAS* data, a suite of space infrared observatories has made ever better use of this window on galaxy evolution. *ISO* obtained the first deep surveys at both mid- and far-infrared wavelengths and pioneered the use of mid-infrared spectra as diagnostics of dusty galaxies. *Spitzer* revolutionized mid-infrared surveys and obtained direct mid-infrared spectroscopy of high-z galaxies. *AKARI* provided uniquely detailed mid-infrared photometric coverage. All these small fully cryogenic telescopes were severely limited by source confusion when aiming for deep surveys in the far-infrared, needed to measure the dominant SED range without uncertain extrapolations. The *Herschel* 3.5 m large mirror has opened the full 70–500 μm range for photometric surveys of unprecendent depth, used by key projects such as HerMES (Oliver et al. 2012), PEP (Lutz et al. 2011), GOODS-Herschel (Elbaz et al. 2011), H-ATLAS (Eales et al. 2010) and the Herschel lensing survey (Egami et al. 2010).

Figure 1 visualizes the current state of deepest far-infrared surveys. Surveys with small 5″ to 30″ beams are now available over the full 24–870 μm range. In the deepest fields, they are confusion limited for all wavelengths except at ~70 μm. Unique future opportunities exist for a 3 m class cryogenic observatory such as SPICA in (i) making a large step in wide and deep mid-infrared surveys (ii) making use of the diagnostic power of the 30–100 μm range in particular for studying the coexistence of AGN and star formation (iii) lifting the limitations that are set by the small areas over which *Herschel* could obtain its deepest 100–160 μm surveys, and most importantly (iv) providing for the first time far-infrared spectroscopy of the typical detected sources, a capability that was out of reach of the *Herschel* passively cooled telescope.

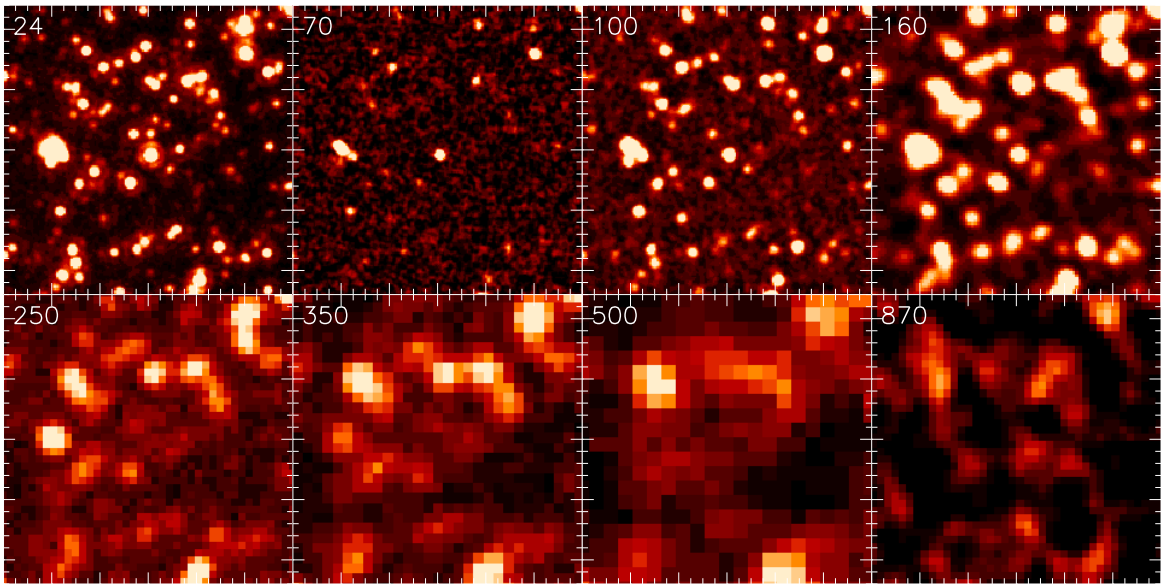

Figure 1. Current status of deepest 24–870 μm infrared surveys, visualized by $4' \times 4'$ cutouts in the HUDF region. Data are from the GOODS project (24 μm), PEP and the combined PEP and GOODS-Herschel data (70–160 μm), HerMES (250–500 μm), and the groundbased LESS survey (870 μm, Weiß et al. 2009).

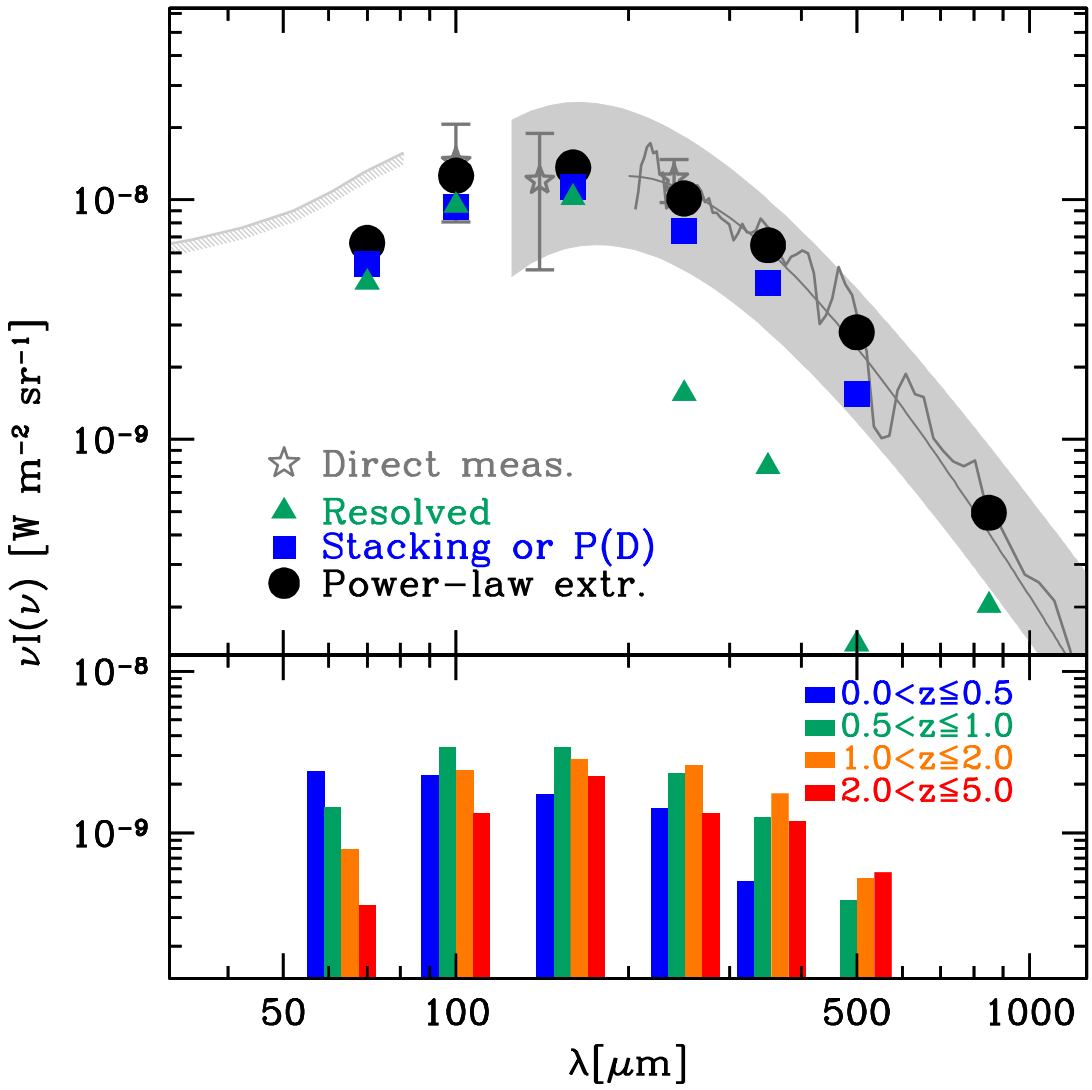

Figure 2. The cosmic far-infrared background as seen by direct measurements and as resolved by *Herschel*. Direct measurements (*grey*) include the γ-ray based limits of Mazin & Raue (2007), *COBE*-DIRBE results as presented in Dole et al. (2006) (*asterisks*), the *COBE*-FIRAS $\lambda > 200\,\mu$m spectrum of Lagache et al. (1999) and the modified blackbody fit of Fixsen et al. (1998). CIB contributions by resolved sources are from Berta et al. (2011) and Magnelli et al. (2013b) (70–160 μm), Béthermin et al. (2012) (200–500 μm) and Zemcov et al. (2010) (850 μm). Stacking results are from Béthermin et al. (2010) (70 μm) Berta et al. (2011) (100, 160 μm) and Béthermin et al. (2012) (250–500 μm), power law count extrapolations from the same works and Zemcov et al. (2010) (850 μm). The lower panel shows the contributions of different redshift slices to the part of the CIB that is contained in resolved sources (PACS) and covered by stacking (SPIRE) (Berta et al. 2011; Magnelli et al. 2013b; Béthermin et al. 2012).

Around three quarters of the cosmic infrared background (CIB) near its peak are now resolved into individually detected sources (Figure 2). The extrapolation of the directly measured counts is consistent with direct CIB measurements, and provides smaller uncertainties at some wavelengths. At longer wavelengths where confusion is more severe, statistical methods can still be applied. In total, *Herschel* provides a quantification of the contribution of different redshift slices to the 70–500 μm CIB.

Using the direct *Herschel* measurements near the rest frame far-infrared SED peak which minimize the uncertainty in deriving the total infrared luminosity of a galaxy, infrared luminosity functions and the contribution of dust-obscured star formation to the cosmic star formation density are now measured out to $z \gtrsim 3$ (Gruppioni et al. 2013; Magnelli et al. 2013b).

2. INFRARED SEDS IN RELATION TO THE MAIN SEQUENCE OF STAR FORMING GALAXIES

Traditionally, studies in the local universe make use of a terminology of 'luminous infrared galaxies (LIRGs)' defined by their total 8–1000 μm infrared luminosity $L_{\rm IR} > 10^{11}\,{\rm L}_\odot$, and their 'ultra-' and 'hyper-' luminous ULIRG and HYLIRG

equivalents above 10^{12} and $10^{13}\,L_\odot$, respectively. These are handy acronyms, but for the purpose of galaxy evolution studies it is important to recall that connotations of these classifications that were carefully calibrated in the local universe may not apply at high redshift. For example, local ULIRGs are found to be major mergers with unusually dense and warm interstellar medium. The same cannot necessarily be assumed for their higher redshift equivalents at same infrared luminosity.

An incarnation of this problem emerged when the rich *Spitzer* mid-infrared surveys were extrapolated to total infrared emission, typically using locally calibrated luminosity dependent spectral templates (e.g. Chary & Elbaz 2001). These libraries encode the physical properties of local infrared galaxies, specifically the lower ratio of 8 μm PAH emission to total infrared for local ULIRGs, which relates to the compact star forming regions and intense radiation fields of these galaxy mergers. Already during the *Spitzer* era, observations suggested that at $z \sim 2$ application of these templates leads to overpredicted IR luminosities (Papovich et al. 2007; Daddi et al. 2007). This 'mid-IR excess' was ascribed to either relatively stronger PAH emission in $z \sim 2$ galaxies, or to a strong AGN mid-IR continuum.

Herschel observations clearly determine this mismatch for large samples and for individual detections. There is a factor ~ 5 overprediction of $z \sim 2$ SFRs if using 24 μm photometry and typical locally calibrated template families (Nordon et al. 2010, 2012; Elbaz et al. 2010, 2011). The effect conspicuously sets in close to $z \sim 2$ when the strongest PAH feature enters the MIPS 24 μm band (Elbaz et al. 2010, 2011), suggesting it is due to enhanced PAH emission rather than to AGN continuum. This is unambiguously confirmed (Nordon et al. 2012) by fully reproducing the photometric trends by trends in the PAH emission in the ultradeep low resolution *Spitzer* spectra of $z \sim 1$ and $z \sim 2$ galaxies by Fadda et al. (2010).

Over the last years, it has been established that most star forming galaxies follow a rather tight (dispersion ~ 0.3 dex) relation between star formation rate and stellar mass, dubbed the main sequence of star forming galaxies. This relation is defined to at least $z \sim 2$ and its normalisation rises steeply with redshift, in line with the increased molecular gas content of high redshift galaxies (e.g. Tacconi et al. 2013). Using a combination of *Herschel* star formation rates for highly star forming systems and optical/UV SFRs at lower star formation rate, Rodighiero et al. (2011) establish that at $z \sim 2$ most cosmic star formation happens on this main sequence. Only $\sim$2 % of galaxies representing $\sim$10 % of the total SFR are in 'starbursts' well above the sequence, which may reflect short merger-induced bursts rather than the steady star formation fed from the cosmic web that must be typical for the main sequence.

For a variety of infrared properties characterising galaxies and their interstellar medium, a picture emerges in which the specific star formation rate offset from the main sequence provides a more consistent and less redshift-dependent description than the traditional way of describing properties of (U)LIRGs by simple IR luminosity (see also Figure 3). The 'mid-IR excess' discussed above relates to the fact that high redshift main sequence galaxies have a similar ratio of mid-infrared PAH to total infrared emission as local main sequence galaxies, despite much higher SFR (Elbaz et al. 2011; Nordon et al. 2012). This ratio can be specified as a function of SFR offset from the main sequence in a redshift independent way. A similar situation occurs for the dust temperature characterising the far-infrared SED peak. At high-z, $T_{\rm dust}$ is lower than in local galaxies of same IR luminosity (e.g. Symeonidis et al. 2013) but can be consistently expressed as a function of main sequence offset (Magnelli et al. 2013a). The differences between low and high redshift seen in the amount of deficit for the [C II] far-infrared line compared to infrared luminosity ($L_{\rm [CII]}/L_{\rm IR}$) largely disappears when plotting against $L_{\rm IR}/M_{\rm H_2}$ (a proxy to main sequence offset) rather than $L_{\rm IR}$ (Graciá-Carpio et al. 2011).

Using *Herschel* and other data to place large numbers of galaxies on the stellar mass — SFR plane out to $z \sim 2$ and then studying their HST morphologies, Wuyts et al. (2011) find main sequence galaxies characterised by large sizes and disk-like Sersic indices. These findings as well as kinematic evidence for high-z (clumpy) disks (e.g. Förster Schreiber et al. 2009) all fit a simple pattern: While a local ULIRG with SFR$\sim$200 $M_\odot$yr^{-1} inevitably is an interacting or merging system with a very compact region of intense star formation, a $z \sim 2$ galaxy of same SFR may be a large clumpy disk supporting this same SFR out of its large gas content.

3. STAR FORMATION IN AGN HOSTS

Given the local relations between black hole mass and host properties as well as the similar cosmic evolution of star formation and accretion, studying the relation of SFR and AGN luminosity in individual high redshift objects is of interest. However, many popular star formation indicators are easily overwhelmed by the AGN emission, in particular for type 1 AGN. The rest frame far-infrared offers the best contrast between host emission and AGN induced emission, and several empirical approaches indicate it to be host dominated for typical high-z AGN, with the exception of systems with particularly large ratios of AGN luminosity and SFR. Given area and depth of *Herschel* surveys, it has been possible to map out average star formation rates for X-ray selected (and other) AGN as a function of redshift, AGN luminosity, and in comparison to stellar mass matched references of non-AGN galaxies (e.g. Shao et al. 2010; Santini et al. 2012; Rosario et al. 2012, 2013b; Mullaney et al. 2012).

Over most of the parameter range studied, there is little correlation between host SFR and AGN luminosity, as might have been expected if major merger triggering of both enhanced star formation and AGN activity would play a dominant role (Figure 4). Such a correlation may be indicated only for luminous AGN at low redshift. The typical SFRs however rise with redshift similar to the rise of the 'main sequence'. Comparison with stellar mass matched samples of star forming and passive galaxies suggests that AGN hosts have star formation rates similar to main sequence galaxies of same redshift and stellar mass, but are less likely to be passive/quenched. The similarity between AGN hosts and star forming galaxies

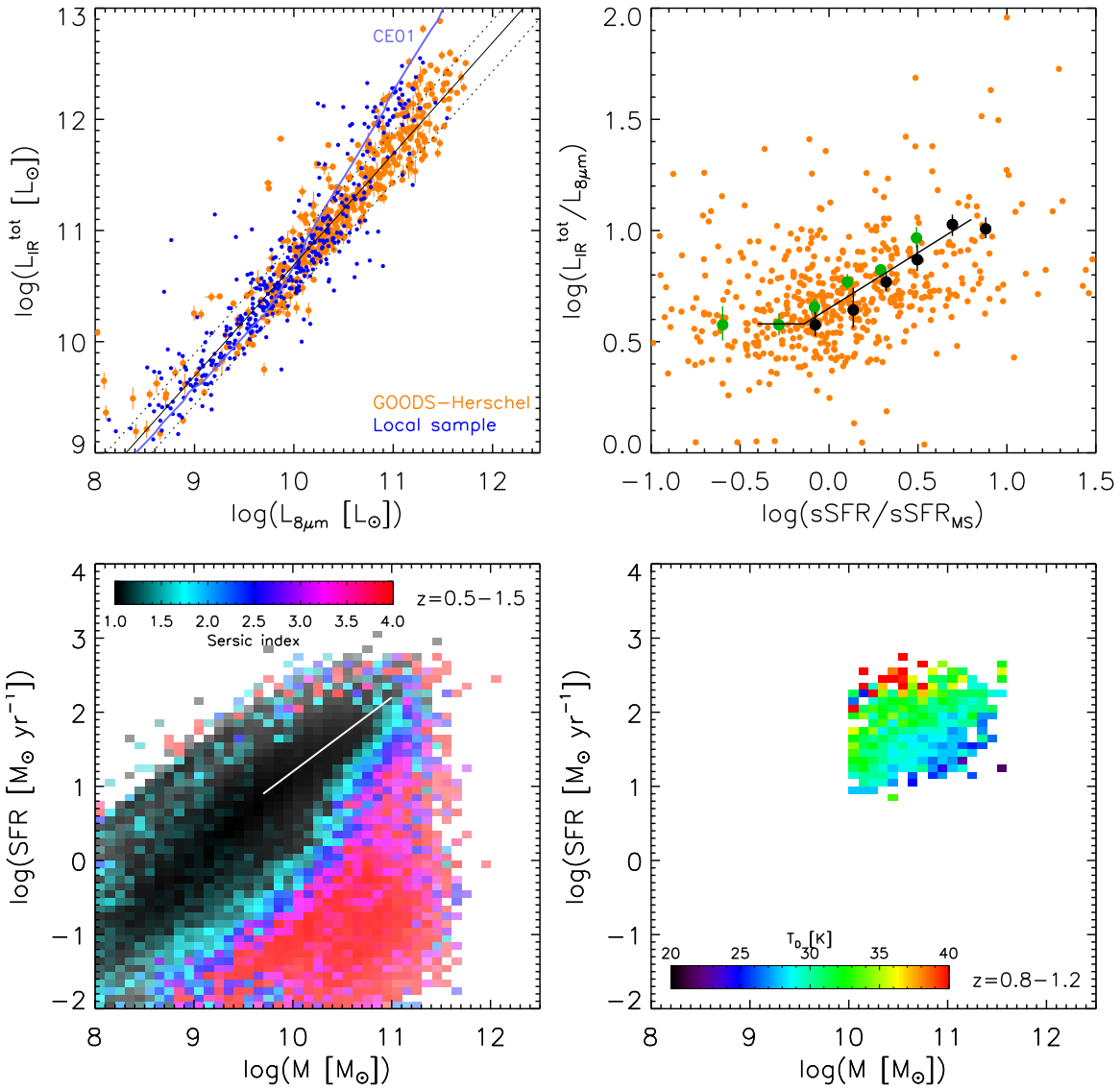

Figure 3. Changes in infrared SEDs of galaxies and their relation to the evolving star forming sequence. *Top left*: Total infrared vs. 8 μm luminosity for a local sample (blue dots) and a $z \lesssim 2.5$ *Herschel* sample (orange dots, diagonal lines visualize median ratio and dispersion for this sample). The blue line shows the locus traced by the Chary & Elbaz (2001) local SED library. Figure adapted from Elbaz et al. (2011). *Top right*: Relation between the offset in specific SFR from the evolving main sequence ('starburstiness') and the ratio of total infrared and 8 μm luminosity. The high-z sample of Elbaz et al. (2011) is shown in orange. Average values from Nordon et al. (2012) are plotted for z∼1 (green) and z∼2 (black), along with their proposed redshift-independent relation (black, their Equation 3). *Bottom left*: Median Sersic indices for galaxies in the $z \sim 1$ star formation rate — stellar mass plane. Low values indicating preference for disk morphologies are found near the main sequence which is qualitatively located by the white line (adapted from Wuyts et al. (2011)). *Bottom right*: Mean temperature of dust in the $z \sim 1$ SFR — stellar mass plane (adapted from Magnelli et al. (2013a)).

of same stellar mass extends to the distribution of rest frame $U - V$ colors (Rosario et al. 2013b). Because of dust, those colors are poor tracers of star formation, however. AGN populate the 'green valley' of a color-mass diagram in a similar way as massive star forming galaxies, and far-infrared based SFR locates many green valley AGN on the main sequence. Location on the green valley then does not correspond to ongoing quenching of star formation. The link between the hosts of moderate luminosity AGN and normal star forming galaxies provided by these *Herschel* studies is fully consistent with the lack of evidence for enhanced merger fractions, in morphological studies of AGN hosts at these redshifts (e.g. Cisternas et al. 2011; Kocevski et al. 2012, and references therein). It is also consistent with the absence of some correlations that are expected in at least some versions of the merger scenario: Obscured AGN as defined by either high X-ray obscuring column or by optical type 2 are not more star forming than unobscured AGN at the same redshift (Rosario et al. 2012; Rovilos et al. 2012; Merloni et al. 2013), and there is no evidence for enhanced star formation in the hosts of those AGN accreting with the highest Eddington ratios (Rosario et al. 2013a).

A picture emerges in which black hole feeding and star formation seem to be connected by the common gas reservoir and gas supply on a long galaxy evolution timescale, and major mergers seem to play a less important role. The shorter

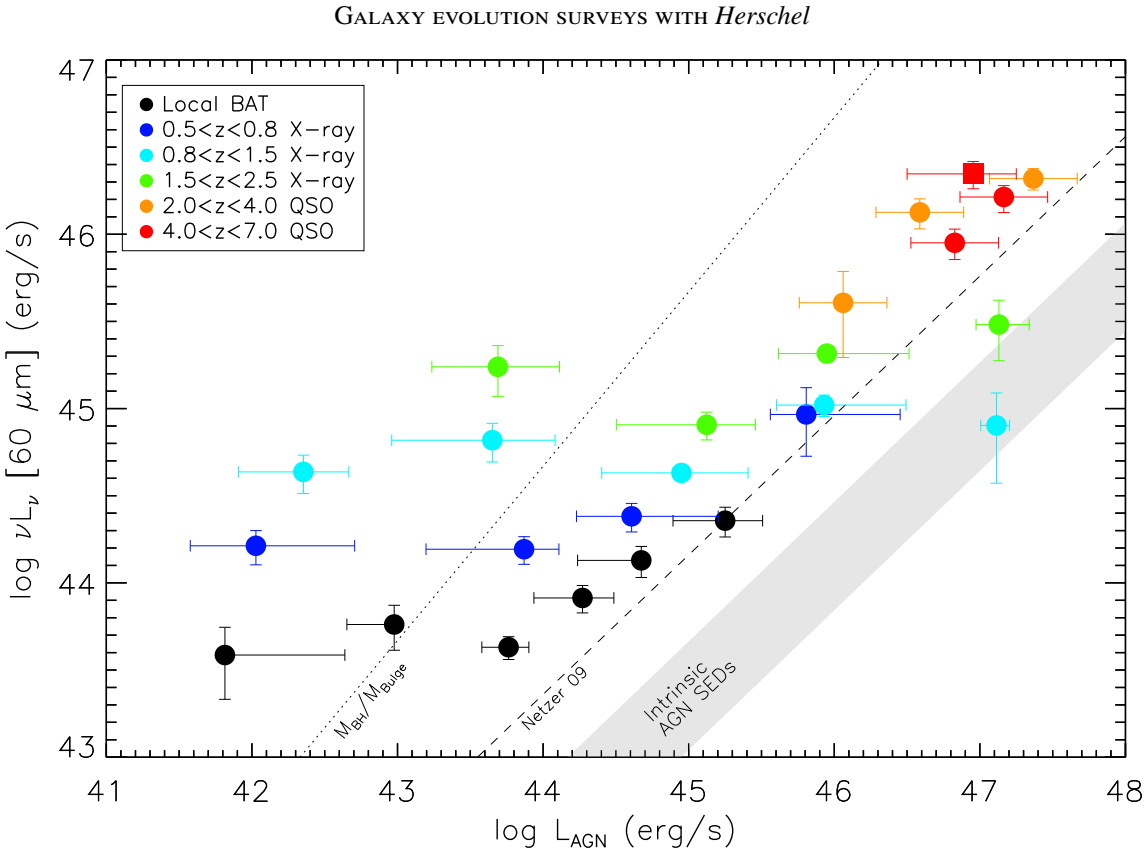

Figure 4. Growth of galaxies and their black holes. Average rest frame far infrared emission of AGN hosts expressing the star formation rate is plotted as a function of AGN luminosity, in different redshift bins. Data for local BAT AGN and for $z < 2.5$ X-ray selected AGN are reproduced from Rosario et al. (2012). Data for optically selected high redshift QSOs are from Serjeant et al. (2010, and priv. comm.) and the z~4.8 sample of Mor et al. (2012, square). Far-infrared luminosities are mean values that include direct detections as well a stacked nondetections. They include all AGN in a bin, and are plotted at the median AGN luminosity with horizontal error bars showing the range including 80 % of the bin's sources. The dotted line indicates the proportionality for a continuous host and black hole growth that would produce the local universe relation between black hole mass and bulge mass (from Häring & Rix 2004, assuming black hole accretion efficiency of 0.1). The diagonal dashed line is the correlation for local AGN-dominated sources as proposed by Netzer (2009), and the diagonal grey band the approximate 1σ range exhibited by empirical pure AGN 'intrinsic' SEDs (see Rosario et al. (2012) for details).

timescales of variations in AGN luminosity compared to variations in SFR are however important in shaping the observed relations, and detailed AGN feeding mechanisms are little constrained.

This contribution reflects the work of many individuals, in particular from the PEP consortium. Special thanks go to Stefano Berta for Figure 2.

REFERENCES

Berta, S., Magnelli, B., Nordon, R., et al. 2011, A&A, 532, A49
Béthermin, M., Dole, H., Beelen, A., & Aussel, H. 2010, A&A, 512, A78
Béthermin, M., Le Floc'h, E., Ilbert, O., et al. 2012, A&A, 542, A58
Chary, R., & Elbaz, D. 2001, ApJ, 556, 562
Cisternas, M., Jahnke, K., Inskip, K. J., et al. 2011, ApJ, 726, 57
Daddi, E., Dickinson, M., Morrison, G., et al. 2007, ApJ, 670, 156
Dole, H., Lagache, G., Puget, J.-L., et al. 2006, A&A, 451, 417
Eales, S., Dunne, L., Clements, D., et al. 2010, PASP, 122, 499
Egami, E., Rex, M., Rawle, T. D., et al. 2010, A&A, 518, L12
Elbaz, D., Dickinson, M., Hwang, H. S., et al. 2011, A&A, 533, A119
Elbaz, D., Hwang, H. S., Magnelli, B., et al. 2010, A&A, 518, L29
Fadda, D., Yan, L., Lagache, G., et al. 2010, ApJ, 719, 425
Fixsen, D. J., Dwek, E., Mather, J. C., et al. 1998, ApJ, 508, 123
Förster Schreiber, N. M., Genzel, R., Bouché, N., et al. 2009, ApJ, 706, 1364

Graciá-Carpio, J., Sturm, E., Hailey-Dunsheath, S., et al. 2011, ApJL, 728, L7
Gruppioni, C., Pozzi, F., Rodighiero, G., et al. 2013, MNRAS, 432, 23
Häring, N., & Rix, H.-W. 2004, ApJL, 604, L89
Kocevski, D. D., Faber, S. M., Mozena, M., et al. 2012, ApJ, 744, 148
Lagache, G., Abergel, A., Boulanger, F., et al. 1999, A&A, 344, 322
Lutz, D., Poglitsch, A., Altieri, B., et al. 2011, A&A, 532, A90
Magnelli, B., Lutz, D., Saintonge, A., et al. 2013a, A&A, in press. (arXiv:1311.2956)
Magnelli, B., Popesso, P., Berta, S., et al. 2013b, A&A, 553, A132
Mazin, D., & Raue, M. 2007, A&A, 471, 439
Merloni, A., Bongiorno, A., Brusa, M., et al. 2013, MNRAS, in press. (arXiv:1311.1305)
Mor, R., Netzer, H., Trakhtenbrot, B., et al. 2012, ApJL, 749, L25
Mullaney, J. R., Pannella, M., Daddi, E., et al. 2012, MNRAS, 419, 95
Netzer, H. 2009, MNRAS, 399, 1907
Nordon, R., Lutz, D., Genzel, R., et al. 2012, ApJ, 745, 182
Nordon, R., Lutz, D., Shao, L., et al. 2010, A&A, 518, L24
Oliver, S. J., Bock, J., Altieri, B., et al. 2012, MNRAS, 424, 1614
Papovich, C., Rudnick, G., Le Floc'h, E., et al. 2007, ApJ, 668, 45
Rodighiero, G., Daddi, E., Baronchelli, I., et al. 2011, ApJL, 739, L40
Rosario, D., Trakhtenbrot, B., Lutz, D., et al. 2013a, A&A, 560, A72
Rosario, D. J., Santini, P., Lutz, D., et al. 2012, A&A, 545, A45
— 2013b, ApJ, 771, 63
Rovilos, E., Comastri, A., Gilli, R., et al. 2012, A&A, 546, A58
Santini, P., Rosario, D. J., Shao, L., et al. 2012, A&A, 540, A109
Serjeant, S., Bertoldi, F., Blain, A. W., et al. 2010, A&A, 518, L7
Shao, L., Lutz, D., Nordon, R., et al. 2010, A&A, 518, L26
Symeonidis, M., Vaccari, M., Berta, S., et al. 2013, MNRAS, 431, 2317
Tacconi, L. J., Neri, R., Genzel, R., et al. 2013, ApJ, 768, 74
Weiß, A., Kovács, A., Coppin, K., et al. 2009, ApJ, 707, 1201
Wuyts, S., Förster Schreiber, N. M., van der Wel, A., et al. 2011, ApJ, 742, 96
Zemcov, M., Blain, A., Halpern, M., & Levenson, L. 2010, ApJ, 721, 424